Turkish Journal of Electrical Engineering & Computer Sciences

http://journals.tubitak.gov.tr/elektrik/

Research Article

Turk J Elec Eng & Comp Sci
(2016) 24: 4957 – 4969

doi:10.3906/elk-1411-63

Effect of transverse magnetic field on low pressure argon discharge

Ehsan HASHEMI*, Kaveh NIAYESH, Hossein MOHSENI
School of Electrical and Computer Engineering, College of Engineering, University of Tehran, Tehran, Iran

Received: 11.11.2014 • **Accepted/Published Online:** 11.10.2015 • **Final Version:** 06.12.2016

Abstract: A numerical simulation was performed to investigate the effect of transverse magnetic fields on low pressure argon plasma. Discovering the variations in electric field, electric potential, power consumption in plasma, and dominant physical mechanisms after application of magnetic fields is the main output of this analysis. A simulation was performed using the finite element method. A 2-fluid model equipped with chemical reaction equations in argon plasma, heat transfer equation, and Poisson's equation was used to describe the plasma behavior. Two disk-shaped electrodes separated by 12 mm from each other were considered as a plasma chamber and an external transverse magnetic field applied. Simulation results show an upset in the electric field after application of a magnetic field. This perturbation is because of the change in particle velocities due to the magnetic field. Changes in electric potential distribution, power loss, and heat transfer procedure are the events described in this paper.

Key words: Electrical discharge, magnetized plasma, circuit breaker, plasma physics, electrical insulation, electromagnetic

1. Introduction

There are several experimental investigations and numerical analyses of magnetic field effects on plasma. This research relies on different applications of low pressure plasma including vacuum circuit breakers (VCBs) and atmospheric arcs, where there are different active gases in each application.

VCBs are the most important application of magnetic fields in interaction with high current plasma in electrical engineering. Commercial VCBs have been taken into account both in numerical and experimental studies. In earlier models, the temperature of plasma is assumed to be constant [1,2] and therefore only specific aspects of plasma could be interpreted by the model. The use of an axial magnetic field to stabilize the high current arc was simulated numerically in [3], where a magnetohydrodynamic (MHD) model of a vacuum arc was developed, which is a single fluid description of plasma. Numerical studies on transverse magnetic field effects on a vacuum arc by using finite element method (FEM) analysis were performed in [4,5]. Both studies simulated the movement of a constricted vacuum arc and its attachment to electrodes by 2 different modeling approaches. The authors of [4] resolved the problem by assuming the arc to be a solid conducting channel, calculating the Lorentz force and then calculating the movement of arc by FEM. In contrast, [5] modeled the plasma affected by the transverse magnetic field by using a MHD model. Both of these investigations dealt with high current ($>$10 kA) plasma and considered magnetic fields in a range of design rules in commercial VCBs, i.e. 10 mT/kA [6].

Extensive experimental investigations were performed in [7,8], where the effects of a magnetic field on

*Correspondence: ehsanhashemi@ut.ac.ir

cathode spot movement and visual plasma situations were reported. An interesting investigation on plasma–magnetic field interaction was performed experimentally to show that plasma voltage could be increased by application of a transverse magnetic field [9]. Experimental results were reported and a simple analytic interpretation was presented to claim that arc voltage increment is high enough to be used for fault current limitation purposes.

This paper presents a 2-dimensional numerical simulation of low pressure argon plasma, 10 mbar, with current of 50 A, which is exposed to a transverse magnetic field, where a 2-fluid model has been taken into account to model the plasma behavior more precisely, which has been used less in previous research. The use of cross-sectional data of electrons in different levels of energy to model the chemical reactions (elastic and ionizing impacts in argon) is considered with respect to the use of commercial FEM software, COMSOL Multiphysics version 4.2. Discussions presented here give the transient phenomena that happen in plasma in the presence of a transverse magnetic field.

2. Physical model

Equations considered in this analysis are continuity, mass conservation, heat transfer, and electromagnetic equations. A summary of these equations will be given in this section [10–16].

$$\begin{aligned} &\tfrac{\partial n_e}{\partial t} + \nabla.\overrightarrow{\Gamma}_e = R_e - (\overrightarrow{u}.\nabla)\, n_e \\ &\overrightarrow{\Gamma}_e = -(\overrightarrow{\mu}_e.\overrightarrow{E})n_e - \overrightarrow{D}_e.\vec{\nabla}n_e \end{aligned} \tag{1}$$

$$\begin{aligned} &\tfrac{\partial n_\varepsilon}{\partial t} + \nabla.\overrightarrow{\Gamma}_\varepsilon + \overrightarrow{E}.\overrightarrow{\Gamma_e} = R_\varepsilon - (\overrightarrow{u}.\nabla)\, n_\varepsilon \\ &\overrightarrow{\Gamma}_\varepsilon = -(\overrightarrow{\mu}_{en}.\overrightarrow{E})n_\varepsilon - \overrightarrow{D}_{en}.\vec{\nabla}n_\varepsilon \quad , \overrightarrow{\mu}_{en} = \tfrac{5}{3}\overrightarrow{\mu}_e \quad , \overrightarrow{D}_{en} = \overrightarrow{D}_e T_e \end{aligned} \tag{2}$$

$$\begin{aligned} &\rho\tfrac{\partial w}{\partial t} = \nabla.\overrightarrow{F_i} + R_a \\ &\overrightarrow{F_i} = \rho w\overrightarrow{V_d} \\ &\overrightarrow{V_d} = D_a^m\overrightarrow{\nabla}\ln(w) + \tfrac{D_a^T}{\rho w}\overrightarrow{\nabla}\ln(T) z u_m \overrightarrow{E} \end{aligned} \tag{3}$$

$$\rho C_P\frac{\partial T}{\partial t} + \rho C_P\,\overrightarrow{u}.\overrightarrow{\nabla}T = \nabla.(k\overrightarrow{\nabla}T) + Q \tag{4}$$

$$\nabla.\overrightarrow{E} = \frac{e(zn_i - n_e)}{\varepsilon_0} \tag{5}$$

$$\overrightarrow{j} = e\,(zn_i\overrightarrow{v_i} - n_e\overrightarrow{v_e}) \tag{6}$$

Eq. (1) is the continuity equation and it describes the number of electrons according to their movement and production rate. In this equation n_e, u, D_e, R_e, μ_e, and E represent number density, convection velocity of fluid, diffusion coefficient, reaction rate of electron production, electron mobility, and electric field, respectively. This equation is used by most researchers in plasma, as in [3,17].

Eq. (2) is the energy conservation equation, which describes electron energy density. In this equation n_ε, D_{en}, and μ_{en} represent electron energy density, electron energy diffusion coefficient, and electron energy

mobility, respectively. R_ε is the energy loss-gain according to inelastic equations between electrons and heavy species.

Eq. (3) is the mass conservation equation for heavy particles. In this equation w, ρ, R_a, D_a^m, D_a^T, z, u_m, and T are mass fraction, fluid density, production rate of heavy species, drift diffusion coefficient, thermal diffusion coefficient, ion charge number, ion mobility, and temperature of heavy species, respectively. Index 'a' represents the type of heavy particle, i.e. neutral atom, positive ion, or excited atoms.

Eq. (4) is the heat transfer equation in fluid. In this equation C_p, k, and Q are heat capacity, thermal conductance, and heat source, respectively.

Eq. (5) is the Maxwell equation for electric field in time invariant conditions. Here, n_i and ε_0 are ion number density and vacuum permittivity, respectively.

Eq. (6) gives the current density flowing through the plasma, in which n_i, e, v_e, and v_i are ion density, electric charge of electron, electron velocity, and ion velocity, respectively.

In this analysis, the collision cross-section values of electrons and Townsend ionization coefficient versus electron energy have been taken into account to calculate reaction rates for all types of particles in different parts of the plasma chamber [13–16]. In addition, the Maxwellian distribution function is assumed to model the electron energy distribution [12]. Considered particles in this analysis are the electron, argon positive ion (Ar+), argon neutral atom (Ar), and Argon excited atom (Ar^*). Chemical reactions that describe the different impacts between electrons, ions, and atoms are given below.

$$e + Ar \Rightarrow e + Ar \text{ (Elastic reaction)} \tag{7}$$

$$e + Ar \Rightarrow e + Ar^* \text{ (Excitation)} \tag{8}$$

$$e + Ar \Rightarrow 2e + Ar^+ \text{ (Ionization)} \tag{9}$$

$$e + Ar^* \Rightarrow 2e + Ar^+ \text{ (Stepwise Ionization)} \tag{10}$$

$$Ar + Ar^* \Rightarrow e + Ar^+ + Ar \text{ (Penning Ionization)} \tag{11}$$

These equations are implemented in commercial FEM software, COMSOL Multiphysics. Notation of formulations is as implemented in COMSOL Multiphysics software [18].

3. Boundary conditions

3.1. Cathode boundary condition

In the set of equations the cathode has been assumed to have a 70% active surface. For analyzed geometry in this research, a disk with radius of 5.5 mm acts as the cathode and the injected electron current density from the cathode to plasma bulk as a function of radius is as assumed in [3]. In a 50 A plasma the arc will be in diffuse mode because of the low value of the magnetic field generated by the arc current. In this situation, connection of the plasma to the cathode has been assumed to be stationary and changes in plasma position occur in the medium.

Secondary electron emission on the cathode surface has been taken into account as the boundary condition for ion and electron densities on the cathode surface. The cathode is assumed to be hot enough to emit electrons

with respect to the electric field of the sheath region. In other words, the cathode emits an electron flux equal to the total current specified by the external circuit of the plasma chamber. Equations describing the behavior of the cathode in an electron flux issue are given below.

$$\overrightarrow{n} \,.\, \overrightarrow{\Gamma}_e = \frac{1}{2} v_{e,th}\, n_e + n_e\,(\overrightarrow{\mu}_e . \overrightarrow{E}).\, \overrightarrow{n} - (\gamma_i(\overrightarrow{n} \,.\, \overrightarrow{\Gamma}_i) + \overrightarrow{n} \,.\, \overrightarrow{\Gamma}_{e,injected}) \tag{12}$$

$$\overrightarrow{n} \,.\, \overrightarrow{\Gamma}_\varepsilon = \frac{1}{2} v_{e,th}\, n_\varepsilon + n_\varepsilon\,(\overrightarrow{\mu}_\varepsilon . \overrightarrow{E}).\, \overrightarrow{n} - (\gamma_i\, \varepsilon_i\,(\overrightarrow{n} \,.\, \overrightarrow{\Gamma}_i) + \varepsilon\, \overrightarrow{n} \,.\, \overrightarrow{\Gamma}_{e,injected}) \tag{13}$$

In Eqs. (12) and (13), $\mathrm{v}_{e,th}$, γ_i, ε_i, ε, $\Gamma_{e,injected}$, and n are electron thermal velocity, secondary electron emission coefficient, mean energy of the ion secondary emitted electrons, mean energy of thermally emitted electrons, total injected electron flux, and normal vector, respectively. Total injected electron flux is determined by the current flowing through the plasma by an external circuit as described later.

The effect of the cathode on positive ions and excited atoms that reach the cathode is described in Eqs. (14) and (15). These equations describe the fact that the cathode provides electrons to neutralize the positive ions and absorbs the excitation energy of excited atoms.

$$Ar^+ \Rightarrow Ar \tag{14}$$

$$Ar^* \Rightarrow Ar \tag{15}$$

In the heat transfer equation, the cathode is made from a bulky material, copper, which receives heat flux from plasma and its temperature rises. Although the medium of the cathode is excluded from the plasma-describing equations, it is considered as a medium in the heat transfer equation. Thus, the cathode surface does not act as a boundary condition in the heat transfer equation.

3.2. Anode boundary condition

The anode considered as a perfect sink for electrons [3]. A perfect sink is a boundary condition in which the total electron flux on the anode is equal to drift and thermal electron fluxes with no sources. In the present study, the temperature of the anode will not increase up to melting point and thus the anode will remain inactive during the process and no heavy species are emitted from the anode. Under these conditions, the anode acts as an electron wall, which provides electrons for positive ions impacting the anode and converts them to neutral atoms. Eqs. (14) and (15) are valid for the anode, too.

In the heat transfer equation, the anode acts as the cathode.

3.3. Boundary conditions of chamber walls

The walls of the plasma chamber act for heavy species based on Eqs. (14) and (15). The effect of the walls on electrons is the same as the anode with the difference that in electrical equations the wall acts as a surface charge accumulator. This effect is described in Eq. (16).

$$\begin{aligned} \tfrac{\partial \rho_s}{\partial t} &= \overrightarrow{n}.\overrightarrow{j_e} + \overrightarrow{n}.\overrightarrow{j_i} \\ \overrightarrow{n} \,.\, \overrightarrow{D} &= -\rho_s \end{aligned} \tag{16}$$

In this equation ρ_s, j_e, j_i, D, and n are surface charge density, electron current density, ion current density, electrical displacement, and normal vector, respectively.

3.4. Initial conditions

The initial conditions of the simulation are described in the Table.

Table. Initial values of simulation.

Parameter	Value
$n_e\,(1/m^3)$	10^{19}
$n_i\ (1/m^3)$	10^{19}
Mean electron energy (V)	2
T (K)	300
p (bar)	10^{-2}
V (V)	0

3.5. Interaction between external transverse magnetic field and low pressure plasma

In this paper the effect of the magnetic field on electron movement has been considered as a change in the mobility tensor of electrons. This tensor is replaced by scalar mobility in the continuity equation. Eq. (17) represents the mobility tensor.

$$\mu^{-1}_{magnetized} = \begin{bmatrix} \mu^{-1} & -B_z & B_y \\ B_z & \mu^{-1} & -B_x \\ -B_y & B_x & \mu^{-1} \end{bmatrix} = \begin{bmatrix} \mu_{xx} & \mu_{xy} & \mu_{xz} \\ \mu_{yx} & \mu_{yy} & \mu_{yz} \\ \mu_{zx} & \mu_{zy} & \mu_{zz} \end{bmatrix} \tag{17}$$

Here $\mu_{magnetized}$, μ, B_x, B_y ,B_z, μ_{xx}, μ_{yy}, μ_{zz}, μ_{xy}, μ_{xz}, and μ_{yz} are the mobility tensor, mobility of an electron in nonmagnetized plasma, magnetic flux density along the x, y, z axes, and elements of mobility tensor, respectively. In this paper an external magnetic field with a value of 20 mT has been applied to the plasma chamber while this field is perpendicular to the current path. In 2D modeling, if the plasma is assumed to be placed in the X-Y plane, the desirable external magnetic field should be on the Z-axis. This magnetic field pushes the plasma to one side of the chamber depending on the magnetic field direction. Cylindrical coordinates and axial symmetry are used in this paper to reach a more convergent solution. By this assumption, movement of plasma to one side of the chamber converts to a concentration or dispersion of plasma.

Values of mobility tensor elements in cylindrical coordinates (r, φ,z) were calculated for different values of magnetic flux density. The results are illustrated in Figure 1.

There are 2 sets of mobility values in Figure 1. The green-black set represents diagonal and nondiagonal elements of mobility sensors when the mobility of electrons is 2000 (m^2/Vs) in the absence of a magnetic field. The blue-red set represents diagonal and nondiagonal elements of mobility sensors when the mobility of electrons is 1000 (m^2/Vs) in the absence of a magnetic field. According to Figure 1, the values of diagonal elements decrease intensely while the values of nondiagonal elements increase primarily and then decrease to a lower value. In higher values of magnetic flux density, greater than 5 mT, the dominant mobility tensors are the nondiagonal ones.

4. Analyzed geometry

The geometry of electrodes considered in this analysis is 2 disk-shaped electrodes with a radius of 5.5 mm separated by 12 mm from each other. An external circuit is assumed to feed the plasma chamber. This circuit includes a DC power supply with amplitude of 1000 V, a current limiting resistor, and a smoothing capacitor

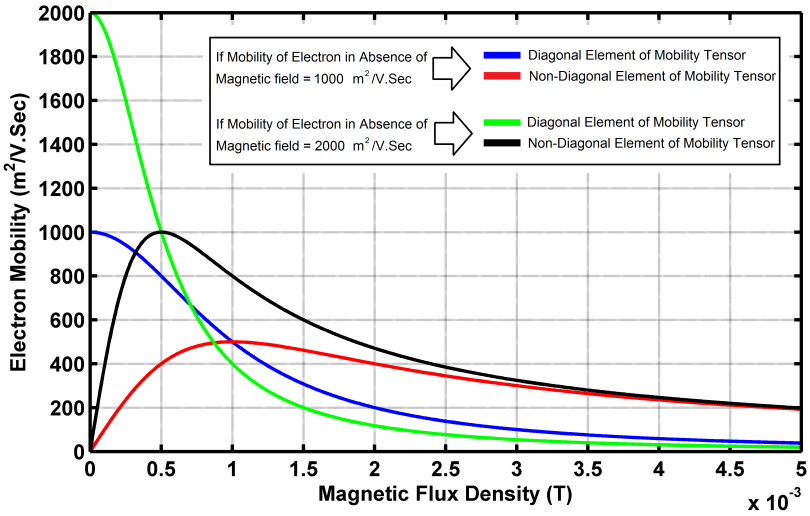

Figure 1. Variation of electron mobility tensor versus magnetic flux density.

with value of 20 Ω and 1 pF, respectively. The smoothing capacitor is placed in parallel with the plasma chamber.

Finite element analysis was performed for the mentioned plasma chamber with a pressure of 10 mbar and a magnetic field of 20 mT, which is much larger than the magnetic field generated by a 50 A current flowing through the plasma chamber. Considered coordinates are cylindrical, and the geometry is assumed to have axial symmetry. The magnetic field has φ-axis direction according to Section 5. The spatial region affected by the magnetic field and the schematic of the external circuit are depicted in Figures 2a and 2b, respectively. Commercial FEM software, COMSOL Multiphysics version 4.2, has been used to perform this analysis.

The main idea for choosing the magnetized region as shown in Figure 2a is an effort to increase the plasma voltage according to [9]. A magnetic field including the anode tries to prevent the electrons from reaching the anode. In an electrical description, this means more resistance and more voltage drop in the plasma.

Required time to reach steady-state conditions before applying the magnetic field is 1 ms. Values of parameters in this time step have been taken into account as the initial condition to calculate the plasma parameters in the presence of a magnetic field.

The temporal behavior of electron density, electron temperature and power dissipation in the plasma chamber, and the plasma temperature are illustrated in following section.

5. Simulation results

Distribution of electron density, temperature of electrons, and power loss are depicted in Figures 3a-3l. After the application of a magnetic field, electrons located inside the magnetized region move to the anode and outside of the magnetized region with less velocity in comparison with the nonmagnetized area. This effect is because of the dramatic change in electron mobility caused by the applied magnetic field. These electrons find their path to the anode by revolving around the anode and reach it from the upper side of the anode. Before application of the magnetic field the electrons have different paths, i.e. they reach the anode from the bottom side, as expected. This procedure is illustrated clearly in Figure 3.

A dramatic change in electron temperature is obvious in Figure 3, too. An increment in electron temperature behind the border of the magnetized region up to 3 eV happens while this temperature inside

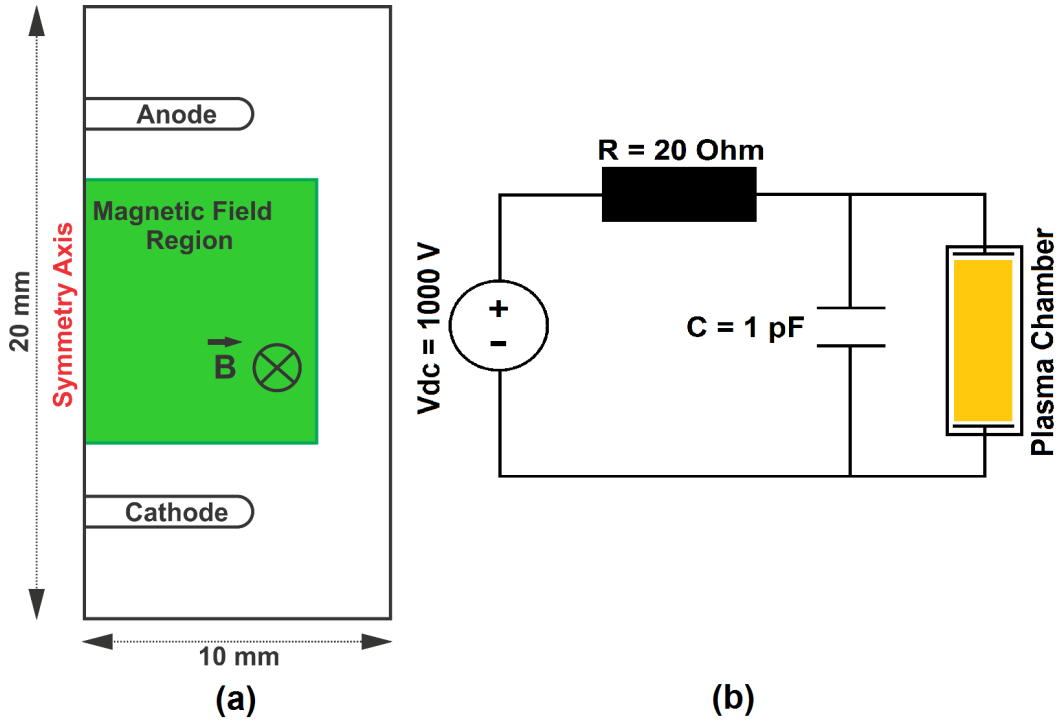

Figure 2. a) Plasma chamber geometry and region of magnetic field. b) Schematic of external circuit.

the magnetized region drops to 0.2-0.3 eV. This variation will affect the thermal characteristics of plasma, discussed in a former section.

An important aspect of the magnetic field effect is the changing of the electric field and consequently the electric potential distribution in plasma. These parameters are shown along the axis of symmetry in the chamber from cathode to anode in Figure 4. The main procedure responsible for changes in the electric field is the separation of positive and negative charged particles due to their change in mobility after application of the magnetic field. In fact, ions respond to the perturbation imposed on plasma by a magnetic field more slowly because of their greater mass and inertia. In addition, the flow path of electrons is changed by the magnetic field and so there is an accumulation of electrons behind the magnetized region. This event is considerable in Figure 3. The pattern of plasma voltage before the application of the magnetic field is in good accordance with results reported in [3]. Space charges are responsible for cathode and anode voltage drops and the similarity between results in this paper and [3] validates the considered physics and equations in this research.

The other important effect of a magnetic field on plasma is causing an upset in the energy transfer procedure in plasma. There is a specific cycle to convert the electric energy to kinetic energy of particles in plasma. This cycle is illustrated in Figure 5. As is known in plasma physics, electrons gain kinetic energy from an electric field according to their mobility and the strength of the electric field. Electrons can have a high level of energy and this energy may transfer to heavy species or low energy electrons by an impact process. Indeed, an energy flux consisting of high energy electrons is emitted from the cathode to the plasma medium, and after passing the sheath area, electrons lose their energy to ions or neutral particles. This process leads to an increment of plasma temperature.

In the middle of this story magnetic fields play a significant role in the energy transfer process. As discussed later, we can describe the effect of a magnetic field by an intense change in electron mobility tensor

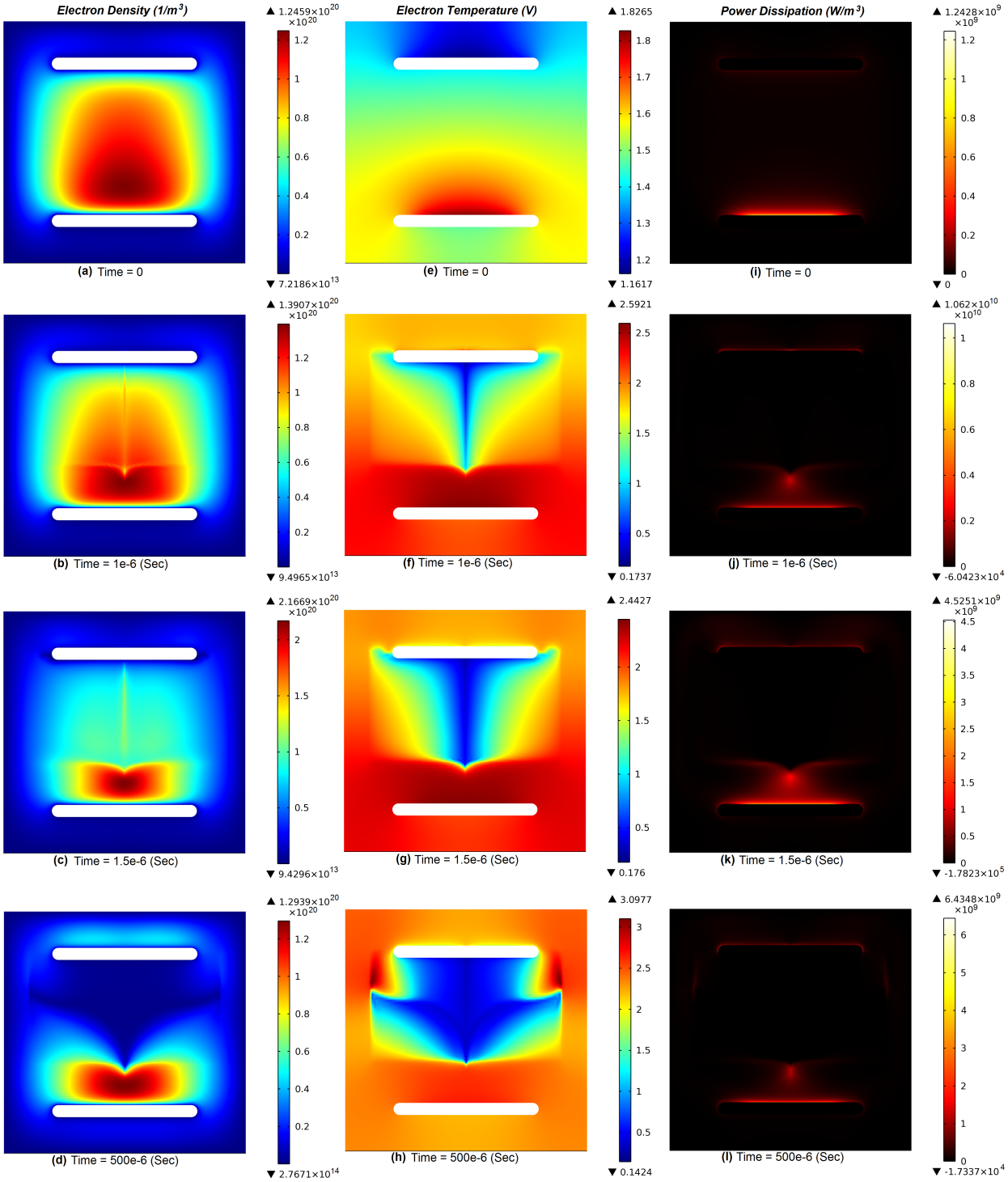

Figure 3. Electron number density ($1/m^3$), electron temperature (V), and power loss (W/m^3) after application of magnetic field in different time steps.

inside the magnetized region of plasma. Electron mobility in the magnetized region is less than that in the nonmagnetized plasma so electrons gain less energy from the electric field in such conditions. In other words,

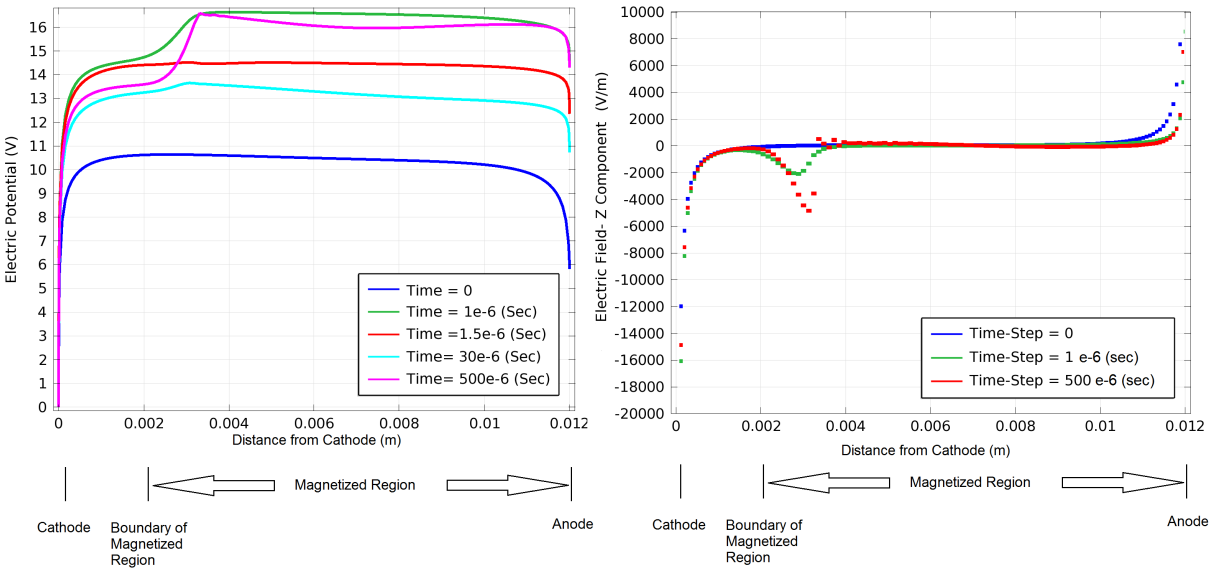

Figure 4. Illustration of electric potential and electric field in different time steps along the symmetrical axis of plasma chamber.

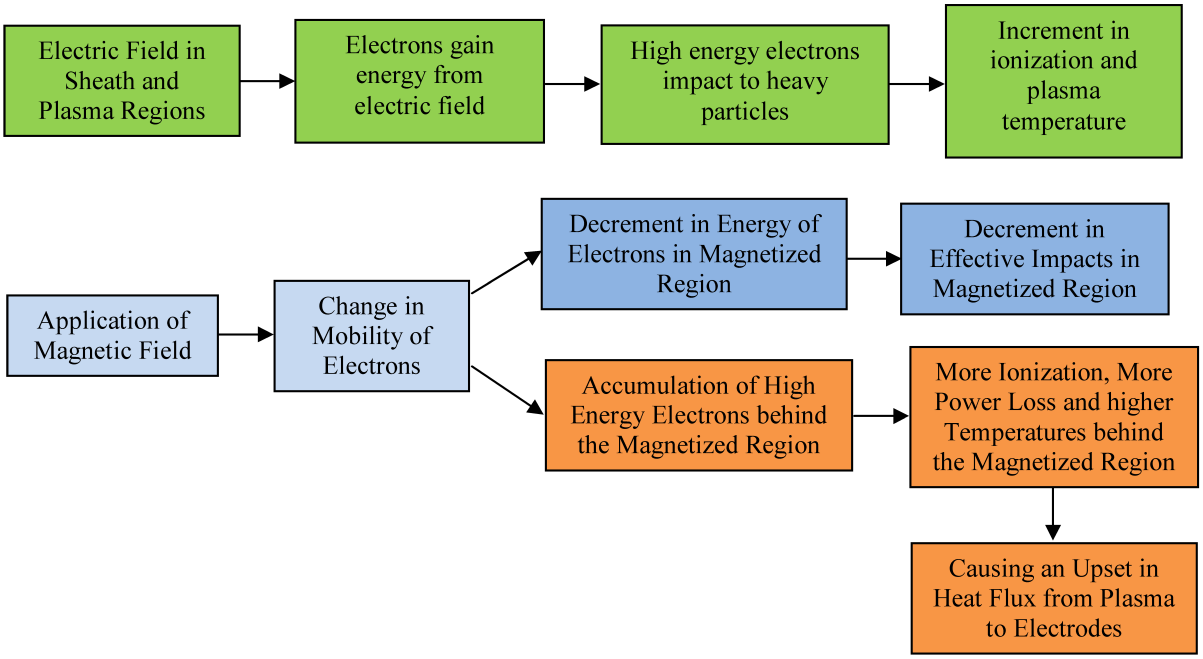

Figure 5. Block diagram describing the effect of magnetic field on energy transfer in plasma.

energy flux decreases because of the reduction of electron velocity. Accumulation of high energy electrons behind the border of the magnetized region causes a high rate of effective impacts between electrons and heavy particles. This mechanism leads to an increasing of the temperature of electrons in such areas. As is known, higher energy electrons cause hotter and more ionized plasma. This physical description also validates the increment of electron density behind the magnetized region. The cycle of energy transfer in magnetized plasma is depicted in Figure 5.

Power consuming processes are ones in which heavy species absorb energy from electrons.

These processes reduce the energy of electrons and in return increase the energy of heavy species and thus the temperature of plasma.

The application of a magnetic field changes the energy gained by electrons in the magnetized region on one hand and causes an upset in the energy flux in nonmagnetized plasma on the other hand. This variation is shown in Figure 3. As a first time step, the main power loss occurs in front of the cathode, where high energy electrons, which gain their energy from the cathode sheath region, face the plasma medium. In the next step another high power loss point appears behind the magnetized region because of the concentration of electron flux in this area. As is obvious in Figure 3, power loss in the magnetized region decreases significantly as the magnetized part of plasma is totally dark in this demonstration.

The final issue, to be discussed in terms of magnetized plasma, is the temperature and total heat flux in magnetized conditions. Figures 6a-6d show spatial variations of plasma temperature and total heat flux in the form of streamlines. Before the application of a magnetic field, the hot spot of the plasma is in the middle of it, but nearer to the cathode. Most power loss in the nonmagnetized plasma is near the cathode, while the hot spot of plasma temperature is relatively far from the cathode. The main reason for this is the role of the cathode as a bulky low temperature mass, which is absorbing a considerable amount of heat flux with no increment in its temperature because of the small time scale of the studied phenomenon. Streamlines of heat flux originate from the hot spot in the plasma and terminate in cold spots. In nonmagnetized plasma, as depicted in Figure 6a, there is only one hot spot in the plasma medium and streamlines originate from this point and reach the cathode and anode surfaces.

Application of a magnetic field causes strong power loss in the down-side and side-wall of the magnetic field region (see Figure 3l). This leads to the gradual appearance of 2 new hot spots in the mentioned points, so the array of streamlines consequently changes, and they originate from the 2 new hot spots and terminate at electrodes as depicted in Figure 6d. This variation in heat flux and temperature should be taken into account to design a low pressure or vacuum plasma system. These hot spots can change the temperature in the solid terms of the chamber, i.e. cathode, anode, and walls.

Figure 7 shows the distribution of total power loss and plasma temperature along the axis of symmetry in the plasma chamber. In the magnetized region, total power loss decreases intensely, by at least 3 orders of magnitude, while this parameter rises behind the magnetic field region. This behavior is illustrated in Figure 7. In another part of Figure 7, the movement of the hot spot toward the cathode is depicted. In nonmagnetized plasma, the hot spot is placed at a distance of 5 mm from the cathode. After 500 μs, the hot spot moves 2.6 mm toward the cathode and the temperature of the hot spot rises from 4932 K to 14,000 K.

6. Conclusion

The influence of a magnetic field on low pressure argon plasma with respect to electric field variations and energy transfer has been investigated in this paper. Important plasma parameters such as electron density, electron temperature, electric potential distribution, power dissipation in plasma, and plasma temperature have been surveyed and the dominant mechanism for observed variations in plasma parameters has been presented.

Most numerical analysis of plasma with the presence of a magnetic field has been done by MHD formulation. In this paper an investigation by a 2-fluid model with detailed chemical reactions in plasma has been performed, which has rarely been considered in the literature. The interesting phenomenon observed in this research is the variations in plasma voltage caused by an external magnetic field. This effect has been reported experimentally but it has not been investigated numerically in as detailed a manner as presented in this paper.

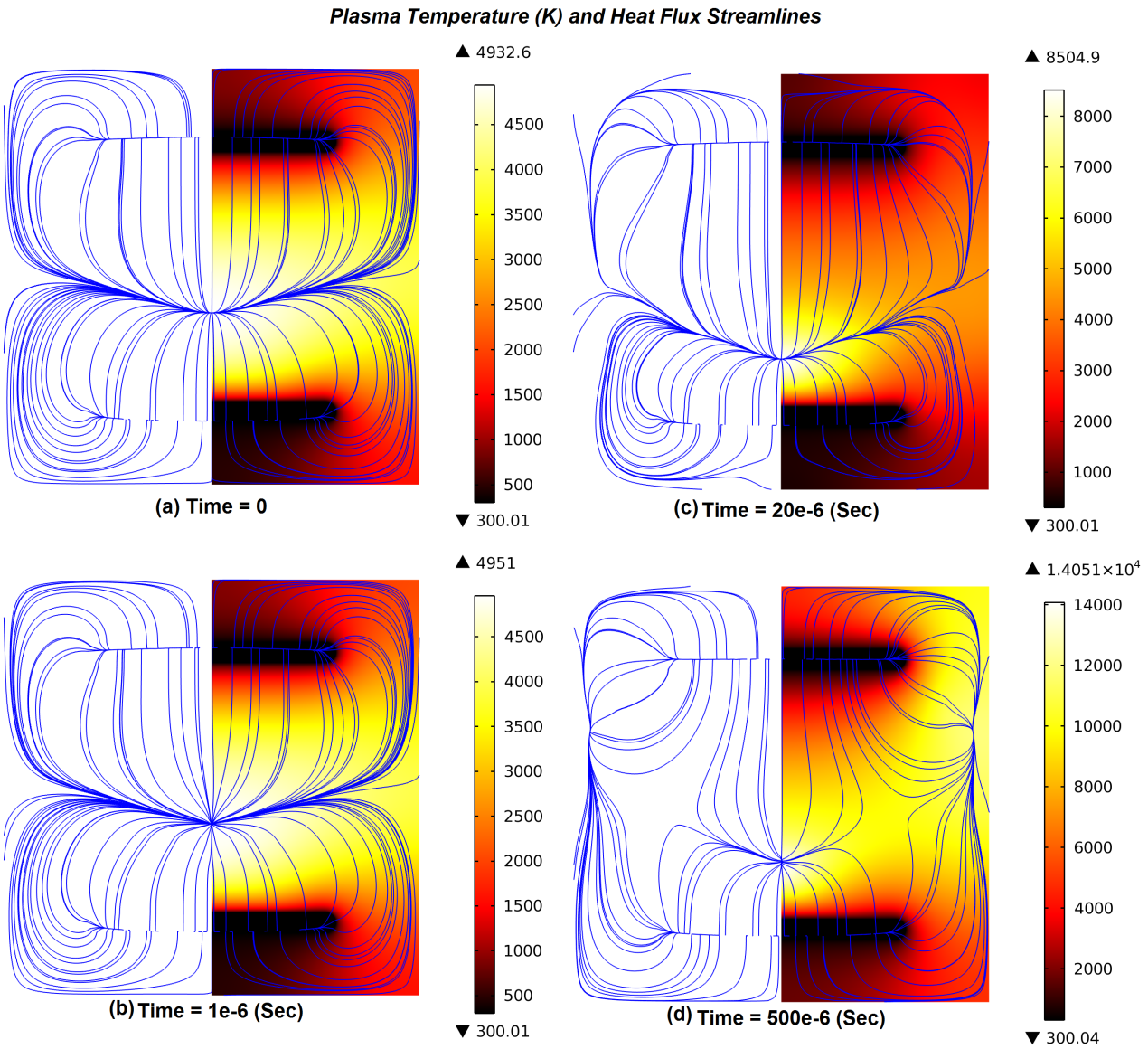

Figure 6. Temperature of plasma (K) and total heat flux (streamlined view) after application of magnetic field in different time steps.

Although this analysis has been performed on a specific geometry under specific plasma conditions, these reported results give major insight to the reader about the effects of a magnetic field on low pressure plasma.

The results presented in this paper show that a relatively strong magnetic field (20 mT) causes a disturbance in the distribution of charged particles, plasma temperature, and heat flux. A considerable increment in the electric field and consequent voltage drop are the interesting effects of a magnetic field on low pressure plasma. Considering thermal issues, the reduction of power dissipation in the magnetized region leads to less heat flux from the plasma to the anode in this geometry. In contrast, power dissipation near the cathode (nonmagnetized region) increases, so it causes more heat flux to the cathode. Both of these phenomena shift the hot spot in plasma, which is illustrated in the presented results.

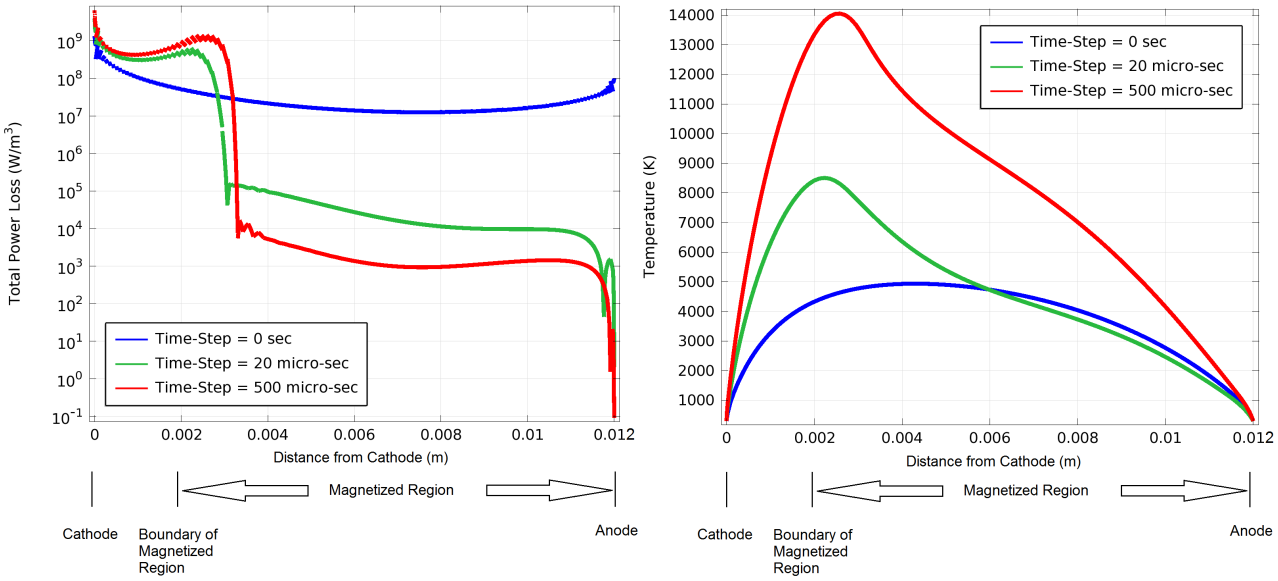

Figure 7. Demonstration of total power loss and plasma temperature along the symmetry axis of the plasma chamber from cathode to anode.

By knowing these dominant mechanisms and their effects, nonconventional applications of magnetized plasma can be realized. As described in Section 1, a fault current limiter can be produced based on increasing arc voltage. If the voltage drop in plasma becomes large enough to be comparable with the voltage of the power network, it will act as an independent fault current limiter. This effect can be the future domain of this research.

Temperature distribution in different parts of plasma can be controlled by the application of multiple magnetic fields. For example, the temperature of the anode surface can be limited to prevent the activation of the anode in low pressure plasmas such as in vacuum arcs in vacuum circuit breakers. The position and amplitude of the magnetic field can be designed by use of the simulation presented in this paper for arbitrary geometries of plasma chambers.

References

[1] Boxman R, Goldsmith S, Izraeli I, Shalev S. A model of the multicathode-spot vacuum arc. IEEE T Plasma Sci 1983; 33: 138-145.

[2] Keidar M, Beilis I, Boxman R, Goldsmith S. Potential and current distribution in the interelectrode gap of the vacuum arc in a magnetic field. In: XVIIth International Symposium on Discharges and Electrical Insulation in Vacuum; 21-26 July 1996; Berkeley, CA, USA. pp. 146-150.

[3] Schade E, Shmelev D. Numerical simulation of high-current vacuum arcs with an external axial magnetic field. IEEE T Plasma Sci 2003; 31: 890-901.

[4] Shmelev D, Delachaux T. Physical modeling and numerical simulation of constricted high-current vacuum arcs under the influence of a transverse magnetic field. IEEE T Plasma Sci 2009; 37: 1379-1385.

[5] Dullni E, Schade E, Shang W. Vacuum arcs driven by cross-magnetic fields (RMF). IEEE T Plasma Sci 2003; 31: 902-908.

[6] Schade E. Physics of high-current interruption of vacuum circuit breakers. IEEE T Plasma Sci 2005; 33: 1564-1575.

[7] Chaly A, Logatchev A, Zabello K, Shkol'nik S. High-current vacuum arc appearance in nonhomogeneous axial magnetic field. IEEE T Plasma Sci 2003; 31: 884-889.

[8] Zabello K, Barinov Y, Chaly A, Logatchev A, Shkol'nik S. Experimental study of cathode spot motion and burning voltage of low-current vacuum arc in magnetic field. IEEE T Plasma Sci 2005; 5: 1553-1559.

[9] Emtage P, Kimblin C, Gorman J, Holmes F, Heberlein J, Voshall R, Slade P. Interaction between vacuum arcs and transverse magnetic fields with application to current limitation. IEEE T Plasma Sci 1980; 4: 314-319.

[10] Surzhikov S, Shang J. Normal glow discharge in axial magnetic field. Plasma Sources Sci T 2014; 23: 054017.

[11] Bellan P. Fundamentals of Plasma Physics. Cambridge, UK: Cambridge University Press, 2008.

[12] Hagelaar G, Pitchford L. Solving the Boltzmann equation to obtain electron transport coefficients and rate coefficients for fluid models. Plasma Sources Sci T 2005; 14: 722-733.

[13] Sam S, Haung S, Freeman G. Electron transport in gaseous and liquid argon: effects of density and temperature. Phys Rev A 1981; 2: 714-724.

[14] Neufeld P, Janzen A, Aziz R. Empirical equations to calculate 16 of the transport collision integrals for the Lennard-Jones potential. J Chem Phys 1972; 57: 1100-1102.

[15] Kee R, Coltrin M, Glarborg P. Chemically Reacting Flow Theory and Practice. New York, NY, USA: Wiley, 2003.

[16] Bird R, Stewart W, Lightfoot E. Transport Phenomena. 2d ed. New York, NY, USA: Wiley, 2002.

[17] Niayesh K, Hashemi E, Agheb E, Jadidian J. Subnanosecond breakdown mechanism of low-pressure gaseous spark gap. IEEE T Plasma Sci 2008; 4: 930-931.

[18] COMSOL Inc. COMSOL Multiphysics 4.2a. User Manual, Plasma Module Theory. Burlington, MA, USA: COMSOL, 2011.